On the Binding Determinants of the Glutamate Agonist with the Glutamate Receptor Ligand Binding Domain

Kirill Speranskiy and Maria Kurnikova*

Chemistry Department, Carnegie Mellon University, Pittsburgh, Pennsylvania 15213

Received March 24, 2005; Revised Manuscript Received June 16, 2005

ABSTRACT: Ionotropic glutamate receptors (GluRs) are ligand-gated membrane channel proteins found in the central neural system that mediate a fast excitatory response of neurons. In this paper, we report theoretical analysis of the ligand−protein interactions in the binding pocket of the S1S2 (ligand binding) domain of the GluR2 receptor in the closed conformation. By utilizing several theoretical methods ranging from continuum electrostatics to all-atom molecular dynamics simulations and quantum chemical calculations, we were able to characterize in detail glutamate agonist binding to the wild-type and E705D mutant proteins. A theoretical model of the protein−ligand interactions is validated via direct comparison of theoretical and Fourier transform infrared spectroscopy (FTIR) measured frequency shifts of the ligand's carboxylate group vibrations [Jayaraman et al. (2000) *Biochemistry 39*, 8693−8697; Cheng et al. (2002) *Biochemistry 41*, 1602−1608]. A detailed picture of the interactions in the binding site is inferred by analyzing contributions to vibrational frequencies produced by protein residues forming the ligand-binding pocket. The role of mobility and hydrogen-bonding network of water in the ligand-binding pocket and the contribution of protein residues exposed in the binding pocket to the binding and selectivity of the ligand are discussed. It is demonstrated that the molecular surface of the protein in the ligand-free state has mainly positive electrostatic potential attractive to the negatively charged ligand, and the potential produced by the protein in the ligand-binding pocket in the closed state is complementary to the distribution of the electrostatic potential produced by the ligand itself. Such charge complementarity ensures specificity to the unique charge distribution of the ligand.

Ionotropic glutamate receptors (GluRs)[1] are agonist-activated cation channels that mediate fast synaptic transmission between neurons. Functioning of glutamate receptors is essential in memory and learning and plays a role in dysfunction of the central nervous system (*1*, *2*). Glutamate receptors are located in the pre- and postsynaptic membrane and are activated by neurotransmitters released from the presynaptic cell. Their natural ligand is glutamate. GluRs are classified according to their signal transduction mechanism into ligand-gated ion channels (ionotropic receptors, iGluRs) and G-protein coupled (metabotropic, mGluRs) receptors. Three major types of ionotropic GluRs are distinguished in accordance with the agonists by which they are activated: *N*-methyl-D-aspartate (NMDA) receptors, α-amino-3-hydroxy-5-methyl-4-isoxazole propionate (AMPA) receptors (GluRl to 4). and kainate receptors (GluR5 to 7 and KA1, KA2) (*1*).

Ionotropic GluRs function as homo- and/or heterotetrameric complexes (*3*, *4*) in which each subunit consists of three transmembrane domains TM1−TM3 and a re-entrant loop, P (see Figure 1a for topology of a GluR). The

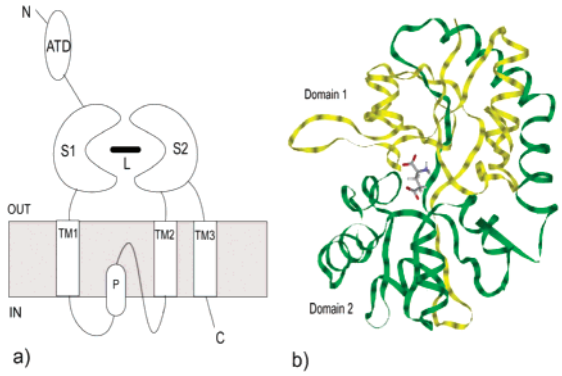

FIGURE 1: General structure of the GluR2 subunit. (a) Topology of GluR2. ATD, amino-terminal domain; S1 and S2 are the two domains forming the ligand-binding site; TM1, TM2, P, and TM3 form the transmembrane region of each subunit; L is a ligand. (b) Ribbon representation of the 3D structure of the S1S2 construct with the glutamate ligand bound to the binding pocket of the protein (*7*). Domain 1 (S1) is shown in yellow; domain 2 (S2) is in green and ligand is shown in CPK colors. In this coloring scheme, carbon is colored gray, oxygen is red, nitrogen is blue, and hydrogen is white.

C-terminal domain of a protein is located intracellularly. The extracellular part of the receptor consists of an N-terminal domain (ATD), thought to play a role in a tetramer association, and a ligand-binding domain (S1S2) (*5*). The ligand-binding domain S1S2 of the GluR2 protein has been expressed as a soluble protein (*6*) and crystallized. Its three-dimensional (3D) structure has been resolved with 1.6−2.0

* Corresponding author. E-mail: kurnikova@cmu.edu; phone: (412) 268-9772; fax: (412) 268-1061.

[1] Abbreviations: GluR2, ionotropic glutamate receptor type 2; MD, molecular dynamics; MD-PBSA, molecular dynamics-Poisson−Boltzmann/surface area; FTIR, Fourier transform infrared spectroscopy; DFT, density functional theory; WT, wild-type protein; PDB, protein data bank; RMSD, root-mean-squared deviation.

10.1021/bi050547w CCC: $30.25
Published on Web 08/02/2005

Å resolution in the presence and absence of agonists and antagonists (*7*−*9*). This protein construct retains ligand-binding agonist/antagonist affinity of an intact receptor and has been extensively studied to characterize ligand−protein interactions of the intact receptor (*6*, *10*−*12*). The sequence alignment of iGluR AMPA subfamily members indicates a high degree of similarity in ligand-binding domains (*9*). The similarity of GluR2 and GluR4 structures is also reflected in kinetic experiments (*12*). Since the binding sites of GluR2 and GluR4 are highly conserved, we used the experimental data obtained for GluR4 S1S2 protein to compare with our results computed for GluR2 protein.

To explain the initiation of the gating of the glutamate receptor ion channels, a "Venus flytrap" mechanism has been proposed (*13*). This reaction involves initial rapid association of a ligand and a protein followed by a slower conformational rearrangement, which results in a structure with the ligand locked deeply in the binding pocket of the protein. According to the proposed mechanism, the ligand first interacts with the side chains of the residues Tyr 450 and Glu 402 of the domain S1. In the second, slower, step, S1S2 changes its conformation and forms a hydrogen-bond network between the ligand and both protein domains S1 and S2 (*9*, *13*).

In this paper, we present detailed theoretical analysis of the ligand−protein interactions in the GluR2 receptor S1S2 ligand binding domain. Crystallographic structures of this protein with several ligands bound in the binding site have revealed that different ligands interact with different subsites in the binding site (*7*, *9*). The structures also show several water molecules near the γ-carboxylate of the glutamate ligand, which may serve as bridges between the protein and the ligand and may play a role in ligand binding. The S1S2 protein has previously been under theoretical investigation (*14*−*19*). For a recent review, see ref *20*. However, much remains unclear about the detailed nature of ligand−protein interactions such as the role of water in the binding site of the protein, as well as role of hydrogen bonds and electrostatic interactions in stabilizing the ligand. In this paper, we investigate agonist−protein interactions in the binding site of the protein and attempt to clarify the role of various factors in ligand specificity and stability. We use molecular dynamics (MD) simulations, continuum electrostatics modeling, and theoretical spectroscopic analysis to investigate agonist−protein interactions and the mobility of water molecules in the protein binding pocket.

One of the most important determinants of ligand binding with GluRs are electrostatic interactions (*10*). Electrostatic charge complementarity of the ligand with its binding site has been a topic of active discussion since the binding site contains a negatively charged side chain of a Glu 705 residue while binding the negatively charged glutamate ligand. In this study, we calculated the electrostatic potential produced by the protein in an open conformation and in a complex with glutamate to demonstrate that while the open unligated GluR2 protein extends positive potential far in the solution (to steer a negatively charged ligand, e.g., glutamate toward its binding site) the electrostatic potential produced by the protein in the closed conformation with the bound ligand does not extend into the solution and at the same time at the surface of the bound ligand it is complementary to the charge distribution of the ligand itself. This result of our study is also in agreement with the recent study of Kubo et al. (*16*) who used a different technique (semiempirical calculations) but came to similar conclusions.

We also present a model of the E705D mutant protein, which is an interesting case because it introduces only a small perturbation in the binding pocket due to mutation of the Glu residue to Asp, yet its affinity to agonist is reduced substantially (*10*). Binding properties of this and similar mutants were previously investigated by mutagenetic biochemical experiments. In these experiments, binding strengths of the full and partial agonists and an antagonist were measured when the Glu 705 residue was substituted with Asp, a polar or a nonpolar residue (*10*, *13*). This mutant has also been under FTIR spectroscopic investigation (*48*). Our results demonstrate that this mutation may induce changes in the hydrogen-bond network in the protein binding site that are critical in ligand recognition and stabilization. Distribution of the electrostatic potential at the surface of the ligand was also found to be different in the ligand and may play a role in weakening its orientational stabilization. However, our calculations of binding energies with the wild-type (WT) and the mutant proteins suggest that the diminished affinity to the ligand in the mutant is due to a larger entropic penalty while electrostatic contribution to the binding energy remains the same in the WT and in the mutant. We provide detailed analysis of these and other observations from our calculations by multiple methodologies in the discussion section of this paper.

MATERIALS AND METHODS

Structure Preparation and MD Simulations. Crystal structures of the GluR2 ligand binding domain (S1S2J) in complex with glutamate (PDB code, 1FTJ) and in the ligand-free state (PDB code, 1FTO) were downloaded from the Protein Data Bank (*21*). We used the residue numbering scheme previously employed by Armstrong and Gouaux (*7*). Under physiological pH conditions, both carboxyl groups of a free glutamate in water are deprotonated and the amine group is protonated. We used ab initio Hartree−Fock method with the 6-31G basis set and the Merz−Singh−Kollman charge fitting algorithm (*25*, *26*) to calculate partial charges on a zwitterionic glutamate molecule. To estimate protonation states of the glutamate bound in S1S2 protein and protein residues in the binding site, we performed pK_a calculations following the procedure of ref *23* implemented in Harlem (*28*), which is based on earlier methods of refs *22*−*24*. All chemical groups were found to have standard pK_a values; therefore, we used standard protonation states and charge distributions from the Cornell et al. force field (*31*).

Crystallographic water molecules within 3 Å of the glutamate ligand, i.e., water molecules 260−264, were retained and labeled W1 through W5, respectively, as in ref *27*. Hydrogen atoms were added to the structure using the program Harlem (*28*). The structure was then solvated in a box of TIP3P water molecules with dimensions 60 × 70 × 65 Å, and periodic boundary conditions were applied. This solvated complex was subjected to the energy minimization followed by a 150 ps MD simulation with constant pressure at $T = 300$ K. The protein and the ligand were restrained by a harmonic force with the force constant 500 kcal/mol. Next, all restraints were removed, and the equilibrium simulation was performed for ca. 500 ps at 300 K under NTV ensemble

conditions. Long-range electrostatic interactions were calculated using the particle mesh Ewald method with a 12 Å cutoff. Bonds involving hydrogen atoms were constrained via the SHAKE algorithm (*29*). The time step for integration was 2 fs, and the coordinates of all atoms were saved every 0.5 ps.

Structure of the E705D mutant was generated by substitution of the Glu 705 side chain for Asp in the WT protein equilibrated in an MD simulation. This mutated structure was equilibrated by running an MD simulation for 100 ps under NTP conditions. Equilibrium trajectory was simulated for 600 ps as an NTV ensemble. Stability of a protein structure in the course of the MD simulations has been assessed by calculating the root-mean-squared deviation of all atoms from the crystallographic structure, which did not exceed 1.5 Å.

To obtain conformations of a free glutamate ligand in aqueous solution, we also performed MD simulations of a glutamate molecule solvated in TIP3P water. After minimization and equilibration under constant pressure, the system was simulated as a NTV ensemble for ca. 1 ns.

All simulations were performed using the AMBER 6 (*30*) software package with the Cornell et al. force field (*31*).

Calculation of Free Energy of Ligand Binding. Calculation of the free energy of ligand-protein binding was performed using the molecular dynamics-Poisson−Boltzmann/surface area (MD-PBSA) approach (*32*). This recently proposed computational method uses equilibrium MD trajectories of a ligand−protein complex and a continuum representation of the water solvent to calculate free energy differences. It has been successfully applied to study DNA−protein, protein−protein, and ligand−protein interactions (*32*−*35*) and interactions of an ion with the ion-channel protein (*36*).

According to the MD-PBSA protocol (*32*), binding energy was calculated as

$$\Delta G = \langle \Delta G_{\text{int}} + \Delta G_{\text{PB}} + \Delta G_{\text{SASA}} - T\Delta S \rangle_0 \qquad (1)$$

where ΔG_{int} is the internal energy contribution to the binding energy, ΔG_{PB} is the electrostatic contribution to the binding energy due to the solvent, ΔG_{SASA} is the nonpolar contribution to the binding energy due to the solvent, and $T\Delta S$ is the change in the solute (ligand) entropy; $\langle\ \rangle_0$ indicates ensemble average over the classical MD trajectory. Each ΔG on the right-hand side of the eq 1 has been calculated as $G^{\text{complex}} - G^{\text{protein}} - G^{\text{ligand}}$, where G^{complex} is the free energy of a protein−ligand complex, G^{protein} is the free energy of a protein, and G^{ligand} is the free energy of a ligand. The internal binding energy was calculated as the difference between internal energy of the ligand−protein complex and internal energies of the protein and the ligand from the same MD trajectory. The nonpolar contribution was calculated using a solvent-accessible surface area (SASA) approach as implemented in the SASA program (*37*). For the continuum electrostatics calculations of ΔG_{PB} binding energy, partial charges for the atoms were taken from the Cornell et al. force field (*31*). The electrostatic energy was calculated via the Poisson equation using the Delphi program (*38*). The grid dimensions of the computational box were 237^3 with the linear scale of ca. 2.5 grid points per angstrom. Dielectric constants of the protein molecule and water environment were taken as $\epsilon_p = 4$ and $\epsilon_w = 79.5$, respectively.

The entropic term, $T\Delta S$, was estimated from the covariance matrix of the ligand positional fluctuations in the MD simulations using the quasi-harmonic approximation as described in detail in refs *39* and *40*.

Calculations of Vibrational Frequencies. To investigate the local ligand−protein interactions, we calculated vibrational frequencies of the ligand carboxylate groups. Frequency of an asymmetric stretch vibration of the carboxylate group is known to be sensitive to the local electrostatic field, and its shift may serve as an indicator of changes in the local environment of this group (*41*, *42*). Our computational methodology was described in detail previously (*43*). In this method, a classical equilibrium MD simulation of the total system solvated in water is performed as described in the *Structure Preparation and MD Simulations* subsection. Next, coordinates of atoms taken from the snapshots of structure from the MD trajectory are used as input for a quantum mechanics program in which the ligand is treated quantum mechanically and the environment is represented via distribution of the partial charges on the protein and water taken from the MD simulation. The positions of atoms that participate in generating the vibration of interest are optimized while the rest of atoms remain fixed at their input value. Quantum mechanical (QM) calculations are performed for several snapshots along the MD trajectory, and the final frequency is found as an ensemble average. We used a cutoff radius of 12 Å for explicit charges (*43*). Calculations were performed using the density functional theory B3LYP/6-31G* level using the Gaussian98 program (*44*). Twenty snapshots were taken from the equilibrated part of the MD trajectory (described above) to calculate average vibrational frequency as

$$\nu = \langle \nu_n \rangle_0 \qquad (2)$$

where $\langle\ \rangle_0$ indicates ensemble average over the classical MD trajectory; υ_n is the frequency calculated for the nth snapshot.

To estimate the effect of a particular protein residue on calculated vibrational frequency, partial charges on this residue were set to zero and quantum mechanical/molecular mechanical (QM/MM) calculations were repeated as prescribed by eq 2. Calculated frequencies were scaled by 0.961 according to the standard convention to obtain better agreement with experimental results (*45*).

RESULTS

Hydrogen-Bond Network and Role of Water in the Protein Binding Site. One goal of this study was to monitor the positions and orientation of water molecules and their "liquidity" in the binding site. We also investigated the geometry and stability of the hydrogen-bond network formed by the ligand in the protein binding pocket. The location of all hydrogen and heavy atoms missing from the crystallographic structure of the GluR2 protein was modeled in the course of the ca. 0.5 ns MD simulations of the WT and the E705D mutant proteins embedded in water solvent (see Materials and Methods). The structure of hydrogen bonds formed by the binding pocket waters observed in the MD simulation is shown in Figure 2, panels a and b show the WT protein and the E705D mutant, respectively. Table 1 lists the average distances between the water oxygens and the C_5-carbon (C_δ) of the ligand in the WT and mutated

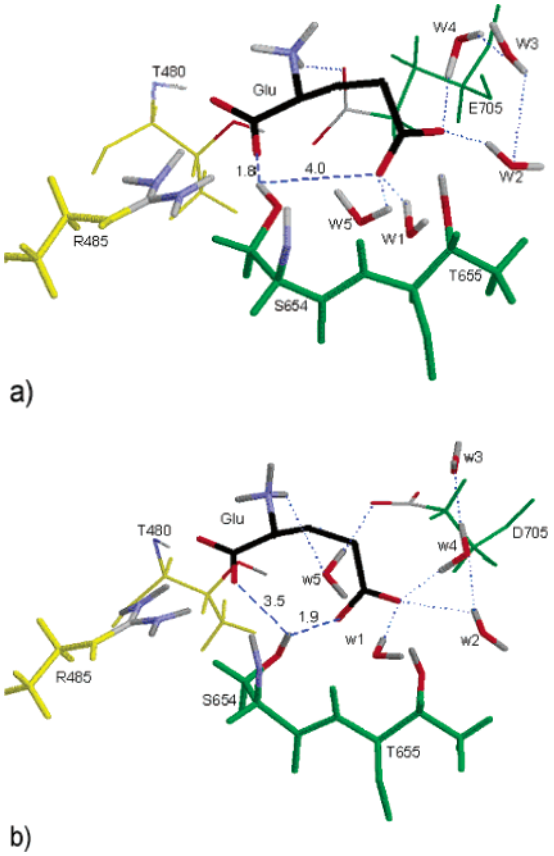

FIGURE 2: Stable positions of binding site water molecules and the Ser 654 side chain in (a) WT protein and (b) mutant E705D binding sites. Distances between Ser 654 hydroxyl group and α- and γ-carboxylates are shown. The ligand γ-carboxyl group interacts with the protein mainly through the water bridges. Ligand hydrogens are not shown to unclutter the picture. The residues of domain S1 are shown in yellow, and the residues of domain S2 are in green.

Table 1: Average Distance and RMSD (Å) between the δ-Carbon of the Glutamate Ligand and Water Oxygens in the Course of the MD Trajectory

	WT S1S2	E705D
C_5−O W1	3.4 ± 0.1	3.3 ± 0.2
C_5−O W2	3.5 ± 0.2	4.4 ± 0.4
C_5−O W3	3.6 ± 0.2	3.6 ± 0.3
C_5−O W4	4.5 ± 0.4	4.6 ± 0.3
C_5−O W5	4.5 ± 0.3	4.0 ± 0.3

proteins as well as the range of their fluctuations. MD results demonstrate the formation of stable water bridges with the γ-carboxylate (C_5OO^-) of the ligand. During the simulation time in the WT protein, four out of five crystallographic water molecules kept their positions near the γ-carboxyl group (see Figure 3). One molecule (W4) diffused out of the binding site during the simulation, but its position near the ligand was immediately occupied by another water molecule that entered the binding site from the bulk.

The E705D mutation affected the positions of water molecules residing in the ligand-binding pocket of the protein. Although all five water molecules remained inside the binding site during the MD simulation of the mutant protein, their positions have changed (see Figure 2b). In the mutant, the four water molecules W1−W4 participated in the stabilization of the γ-carboxyl group. The fifth water molecule, W5, moved into a new stable position to establish

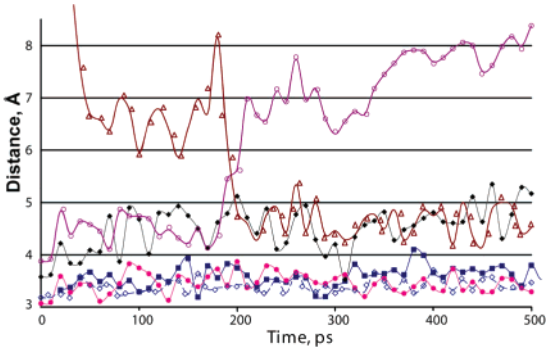

FIGURE 3: Distances between the C_5-carboxyl carbon (C_δ) and oxygens of water molecules, which hold their positions in the binding site of the WT protein, are shown as a function of time from the MD simulations. Water molecules are named as in ref *7* and as shown in Figure 2. W1−C_5 distance is shown with open diamonds; W2−C_5 is filled circles; W3−C_5 is filled squares; W5−C_5 is filled diamonds. The open circles line is the trajectory of water W4, which exchanges its position with a bulk water molecule at approximately 200 ps (open triangles).

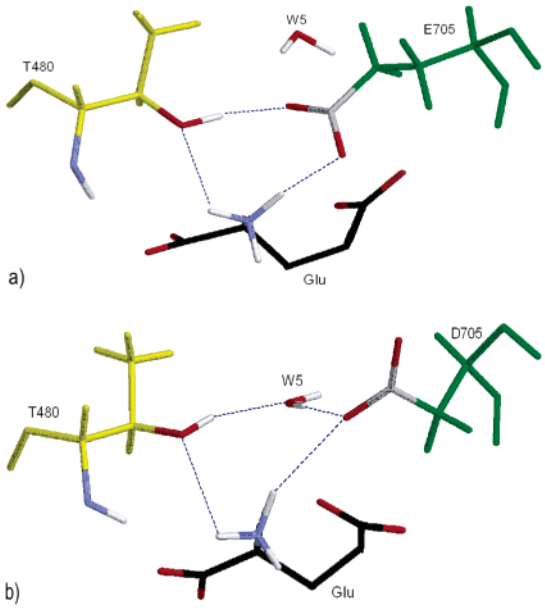

FIGURE 4: Formation of hydrogen bonds between the NH_3 group of the ligand and Thr 480 and Glu 705/Asp 705 of a protein in (a) for the WT protein and (b) for the mutant E705D protein. In the binding site of the WT protein, the ligand interacts directly with the Glu 705 residue. In the mutant, the water W5 forms a bridge between the ligand and the shorter Asp 705 residue. The residues of domain S1 are shown in yellow and the residues of domain S2 are in green.

hydrogen bonds between the ligand HN_3 group and two residues, Asp 705 and Thr 480 (see also Table 1).

During the simulation, a number of hydrogen bonds formed directly between the WT protein and the ligand. The α-carboxyl group (C_1OO^-) formed two strong hydrogen bonds with the positively charged Arg 485 residue. In addition, α-carboxyl formed hydrogen bonds with the NH group of Thr 480 and the NH and OH groups of Ser 654. As shown in Figure 4a, the α-amino group of the ligand was stabilized by interactions with the backbone carbonyl oxygen of Pro 478, the hydroxyl of Thr 480, and the carboxylate oxygen of Glu 705. The γ-carboxyl group formed a direct hydrogen bond with Thr 655. It also formed hydrogen bonds with all four water molecules, which additionally tethered it to the protein.

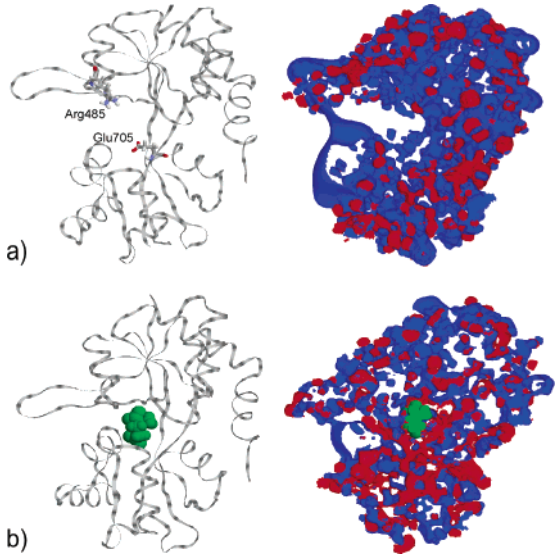

FIGURE 5: Ribbon representation and electrostatic potential isopotential surfaces at 1.5 kcal/mol (a) ligand-free WT S1S2 and (b) the glutamate-bound WT S1S2. Residues Arg 485 and Glu 705 are shown in stick representation. Glutamate ligand is in green space-fill representation. Shown are the isopotential surface slices through approximately the center of the ligand-binding pocket of the protein. Blue is for positive potential, and red is for negative potential.

Table 2: Average Distance and RMSD (Å) between Ser 655 Hydroxyl Hydrogen and the Glutamate Ligand α- and γ-Carboxyl Oxygens Calculated along the MD Trajectory

	Ser 655−O α-carboxyl	H Ser 655−O γ-carboxyl
WT S1S2	1.8 ± 0.1	4.0 ± 0.3
E705D	3.5 ± 0.4	1.9 ± 0.4

Most hydrogen bonds in the binding site of the E705D mutant remained the same as in the WT protein. In particular, residues Arg 485, Thr 480, Pro 478, and Thr 655 formed hydrogen bonds with the glutamate ligand as in the WT protein, and their relative positions did not change dramatically (compare Figure 2, panels a and b). However, the hydroxyl side chain of Ser 654 adopted a different conformation in the mutant, forming a hydrogen bond with the γ-carboxyl group of the ligand instead of a hydrogen bond with the α-carboxyl of the ligand as in the WT protein. See Table 2 and Figure 2 for distances between corresponding atoms in the WT and mutant proteins. Interactions involving the amino group of the ligand also differed in the WT and the mutant. The direct hydrogen bond between the Glu 705 residue and the amino group of the ligand present in the WT protein is no longer possible in the E705D mutant due to the shorter side chain of aspartate. Instead, as mentioned above, the water molecule, W5, formed hydrogen bonds in the center of a triangle formed by the NH_3 group of the ligand, the hydroxyl group of Thr 480, and the carboxyl group of Asp 705, as shown in Figure 4b, thus facilitating Asp 705−Thr 480 interaction.

Electrostatic Potential. Ligands of S1S2 protein are charged molecules; thus, electrostatic interactions are expected to play an important role in protein selectivity and ligand-binding properties. To clarify the role of electrostatic complementarity in ligand binding, we analyzed the electrostatic profiles of S1S2 protein and its mutant in the ligand-bound and ligand-free forms. Calculations were performed with the continuum electrostatics model as described Materials and Methods. Figure 5 shows two-dimensional slices of the equipotential surfaces of the electrostatic potential by the protein made through the binding pocket of the protein in the ligand-free (Figure 5a) and the glutamate-bound (Figure 5b) forms. The 1.5 kcal/mol positive isopotential surface in Figure 5a (ligand-free protein) is located near both positively charged Arg 485 and negatively charged Glu 705. Binding of the negatively charged glutamate ligand changes the electrostatic profile in the binding cleft (Figure 5b); the central part of the protein exhibits mostly negative electrostatic potential when the ligand is bound. Figure 6 shows the isopotential surfaces of 0.5, 1.1, and 1.5 kcal/mol with the different from Figure 5 view to the ligand-binding site. The weakest isopotential surface of positive 0.5 kcal/mol extends substantially into the solution. At this value of the electrostatic potential, it can be "felt" by a negatively charged molecule. The gradual increase of electrostatic potential toward the mouth of the binding site opening is clearly pronounced (see 1.1 and 1.5 kcal/mol equipotential surfaces also shown in Figure 6). Note that the negative potential (shown in Figure 6 by several shades of red) does not significantly extend beyond the boundary of the protein and is not pronounced in the binding site itself. The 1.5 kcal/mol level of the positive potential is located approximately at the surface of the protein atoms lining the ligand-binding cavity.

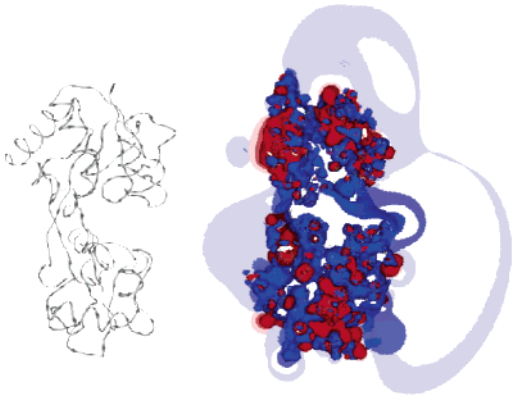

FIGURE 6: Ribbon representation and isopotential surfaces of electrostatic potential of the ligand-free S1S2. The view is rotated with respect to the view in Figure 5. Blue is positive potential and red is negative potential. The lightest shadow is the isopotential surface of 0.5 kcal/mol, medium dark is 1.1 kcal/mol, and dark is 1.5 kcal/mol.

To reveal the charge complementarity between the protein and its ligand, we calculated the electrostatic potentials at the surface of the bound ligand exhibited by the S1S2 protein and the E705D mutant in their closed state (ligand-bound conformation). Thus calculated electrostatic potentials are shown in Figure 7a,c (the ligand molecule is superimposed in Figure 7a to guide the eye). Note that both the WT and the mutant produced positive potentials at the surface of both carboxylates of the ligand and a negative potential at the position of amino group of the ligand (see Figure 7a,c). Next, we removed partial charges from the negatively charged Glu 705 and Asp 705 residues in the WT and mutant structures, respectively (see Figures 7b,d). The removal of charges from the negatively charged Glu/Asp 705 residue significantly reduced the negative electrostatic potential at the surface of

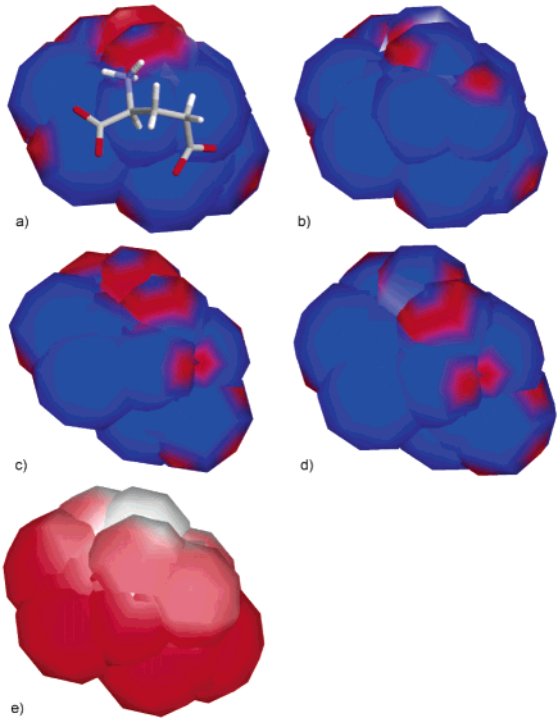

FIGURE 7: Ligand surface colored by the electrostatic potential generated by a protein. Electrostatic potential has been calculated with the ligand removed from the binding pocket; protein is in the ligand bound conformation. Blue is positive potential, red is negative potential, and white is neutral potential. Ligand is shown (a) in the stick representation. (a) Ligand bound to the WT protein; (b) same as (a) but with zero partial charges on the Glu 705 residue; (c) ligand bound to the E705D mutant; (d) same as (c) but with zero partial charges on Asp 705 residue. (e) The electrostatic potential of the ligand itself solvated in water.

Table 3: Experimental and Calculated Protein−Ligand Binding Energy, kcal/mol

	WT	E705D
experimental GluR2 (*12*)	-8.62 ± 0.28	
experimental GluR4 (*13*)	-8.53 ± 0.06	-6.14 ± 0.17
calculated	-12.98 ± 3.91	-8.16 ± 3.77
calculated with no partial charges on		
α-carboxyl ligand group	−0.69	4.01
γ-carboxyl ligand group	−1.13	4.82
α-amino ligand group	−6.93	−5.26
water W1−W5	−3.50	−1.98
Arg 485	0.09	5.80
Glu 705 (or Asp 705)	−14.81	−9.09
Ser 654	−8.91	−1.51
Thr 655	−7.14	−1.72

the amino group of the ligand. However, it is clear from this picture that other protein sites also contribute to the negative potential at this position.

Binding Energy. The calculated binding affinity of the ligand to the WT and the mutant proteins as well as the corresponding experimental values for the GluR2 and GluR4 proteins are reported in Table 3. Our results correctly predict stronger binding of the glutamate with the WT than with the E705D mutant. Calculated absolute binding energies are somewhat overestimated with respect to the experimental results; however, such discrepancy is expected (and turned out to be smaller than expected) considering that the binding energy calculations are very sensitive to the accuracy of the model. In this case, our goal was not to achieve an ideal numerical correspondence with the experimental values but rather to capture the main effects that contribute to the binding energy of the glutamate and compare its binding to the WT protein and its mutant E705D. This mutation preserves the main features of the electrostatics in the binding site, perturbing it only slightly by shifting the negatively charged carboxyl group away from the center of the binding site. Given the simplicity of our free energy calculations the results compare well with the experimental numbers. We can partially attribute the systematic discrepancy in the experimental and calculated absolute energies to the fact that the reorganization energy of the protein upon closing was not taken into account.

The difference in the calculated binding energies for the WT and mutant proteins is mainly due to the difference in the entropic penalty upon ligand binding. The entropic contribution $\langle T\Delta S\rangle_0$ (eq 1) is −14.72 kcal/mol for the WT protein and −20.32 kcal/mol for the mutant. The other terms contributing to the binding energy were similar in both proteins. The nonpolar binding energy was $\langle \Delta G_{SASA}\rangle_0 = -2.5 \pm 0.2$ kcal/mol for both the WT and the mutant proteins, and the electrostatic contribution $\langle \Delta G_{PB}\rangle_0$ was ca. -14 ± 2 kcal/mol.

The relative contribution to the calculated binding energies of various local interactions in the binding site was also estimated. Table 3 summarizes the calculations performed by removing various groups of interactions between a protein and a ligand. As seen in Table 3, the water molecules W1−W5 in the binding site play a significant role in stabilizing the γ-carboxylate of the ligand in the WT protein. In the absence of five bound water molecules, a significant reduction in binding energy is observed for both the WT and the mutant structures (Table 3). Note, also, that in the absence of water, binding of the agonist is more strongly affected in the WT protein, indicating that in this case bound water plays a more important role. The complexes with zeroed out charges on either of the carboxyl groups of the ligand are strongly destabilized. The α-carboxyl group of the ligand forms two hydrogen bonds with the Arg 485 residue. The removal of partial charges from positively charged Arg 485 has approximately the same effect as when α-carboxyl charges are removed from the ligand. The removal of charges from the Thr 655 residue, which forms a direct hydrogen bond with the γ-carboxyl group, has approximately the same effect on the binding energy in both proteins, destabilizing binding by about 6 kcal/mol. Ser 654 forms different hydrogen bonds in the WT and mutant protein structures (see Figure 2). Its absence destabilizes the WT protein complex by ca. 4 kcal/mol and the mutant complex by ca. 6.5 kcal/mol, indicating its stronger contribution to the ligand binding in the mutant.

In the E705D mutant, the α-amino group of the ligand contributes less to the ligand binding than it does in the WT protein. In the absence of this group, the change in ligand binding energy is ca. 6 kcal/mol for the WT and ca. 3 kcal/mol for the mutant. Peculiarly, the removal of the negatively charged Glu 705 or Asp 705 residue, which interacts directly with the ligand's NH_3 group, produced a stabilizing effect in both systems; namely, the calculated ligand affinity increased slightly (Table 3) due to the overall better interaction with the ligand carboxylate groups.

Vibrational Spectra. Calculated and experimentally measured (*46*−*48*) asymmetric stretch vibrational frequencies of

Table 4: FTIR Measured (*46*−*48*) and Calculated in This Work Asymmetric Stretch Vibration Frequencies of the Glutamate Ligand α- and γ-Carboxylates, cm^{-1}

ligand environment	C_1OO^-		C_5OO^-	
	exp	calc	exp	calc
D_2O	1614	1635.2 ± 12.4	1565	1589.5 ± 15.9
WT S1S2	1610	1628.8 ± 9.8	1575	1600.0 ± 8.7
E705D	1609	1626.1 ± 10.9	1560	1573.1 ± 15.0

Table 5: Calculated Shift in Asymmetric Stretch Vibrational Frequencies of the Glutamate α- and γ-Carboxylates upon Zeroing out of Partial Charges on a Particular Protein Residue, cm^{-1}

no partial charges on	C_1OO^-		C_5OO^-	
	WT S1S2	E705D	WT S1S2	E705D
Arg 485	51.3	60.9	−8.3	−7.1
Ser 654	−1.0	1.0	1.4	24.4
Glu 705/Asp 705	27.6	19.8	14.7	20.2

α- and γ-carboxylates in D_2O and GluR4 protein are listed in Table 4. In the experiment when the ligand was bound to the WT protein, the frequency of C_1OO^- is downshifted by 4 cm^{-1} with respect to a free glutamate in D_2O solution. It is downshifted by 5 cm^{-1} when glutamate is bound to the GluR4/E705D mutant. The C_5OO^- band is upshifted by 10 cm^{-1} in the WT protein and it is downshifted by 5 cm^{-1} in the GluR4/E705D mutant.

Each calculated value in Table 4 is the average of 20 single calculations (see eq 2) performed as discussed in Materials and Methods and in detail in ref *43*. Calculated frequencies closely reproduce the experimental results (the absolute difference in 25 cm^{-1} constitutes less than 2% error; see also the extensive discussion in ref *43*). Although binding sites of the GluR2, GluR4, and GluR0 proteins are largely conserved, the observed ligand frequency shifts upon binding to, for example, GluR0 and GluR4 differ slightly and may be indicative of small variations in the ligand environment in the binding site. For example, the observed shift upon transfer of the glutamate from D_2O solution to GluR0 protein for C_1OO^- asymmetric vibration is approximately 2 and 3 cm^{-1} for C_5OO^- (*47*). Small differences between the experimental and the corresponding predicted frequency shifts in the WT and mutant proteins are within experimental and theoretical error and may be due to either small structural differences between the GluR2 and the GluR4 proteins, insufficient sampling, or other approximations made in the theoretical model (for detailed analysis of the theoretical method, see ref *43*).

Table 5 shows calculated C_1OO^- and C_5OO^- vibrational frequencies with zero partial charges on several protein residues nearest to the ligand. For most residues located in the binding pocket, deletion of partial charges from a given residue near ligand carboxylates produced similar effects on frequencies in both the WT and the mutant proteins. However, zeroing out the charge on Ser 654 increased the frequency of the C_5OO^- bound to the mutant by 24.4 cm^{-1} and only by 1.4 cm^{-1} in the WT protein. This result strongly suggests that the downshift of C_5OO^- frequency upon mutation experimentally observed resulted from the formation of a new hydrogen bond between the Ser 654 hydroxyl hydrogen and the ligand C_5OO^- oxygen.

DISCUSSION

To elucidate specific details of the ligand−protein interactions, we performed theoretical analysis of the glutamate ligand binding to the binding pocket of the GluR2 receptor. One unique aspect of this work is that our theoretical model was validated via direct comparison with experimental data. Also, we employ several theoretical methodologies to study the importance of various local interactions in the protein binding site from several perspectives. Calculated vibrational frequencies of the glutamate ligand in solution and when bound to a protein compared exceptionally well with recent FTIR spectroscopic measurements (*43*, *46*−*48*), giving us confidence in the proposed model and in the interpretation of our observations.

Hydrogen atoms are modeled explicitly in MD simulations; therefore, exact directionality and strength of hydrogen bonds forming upon binding of a ligand can be elucidated in the model, supplementing X-ray structural data (*7*) and indirect FTIR analysis (*46*−*48*). In our simulations, the ligand and the protein form a number of stable direct and water-bridged hydrogen bonds. The MD simulations clearly demonstrate that water molecules surrounding γ-carboxylate are important in ligand binding because they provide bridging hydrogen bonds between the ligand and the protein. Quite differently, the α-carboxylate of the ligand forms several direct hydrogen bonds with the protein.

Binding site water molecules participate in the rearrangement of interactions in the E705D mutant protein and may play a role in ligand accommodation during binding and release of the ligand. The simulations show that the α-carboxylate and α-amino groups can be responsible for ligand recognition because they become largely desolvated and bind directly to the protein, while γ-carboxylate remains solvated with water. Most notably, two hydrogen bonds are formed with the NH_2 groups of the Arg 485 residue. As previously observed in kinetic experiments on mutants (*10*, *49*), the mutation of the Arg 485 residue leads to complete loss of the channel function; thus the presence of this group is important for ligand binding. Our calculations of binding energies (see Table 3) and vibrational frequency analysis (see Table 5) strongly support these observations. At the same time, the binding of the ligand, which retains part of its first solvation shell, requires displacement of fewer waters from the binding site and may be an energetically easier process.

We demonstrated that the structural features of the agonists are dictated by the electrostatic potential profile in the GluR2 binding pocket. All glutamate receptor agonists exhibit a specific structural pattern characterized by two negatively charged chemical groups and one positively charged group. The electrostatic potential profile generated by the protein at the surface of the bound ligand (as shown in Figure 7) in the closed cleft conformation (the agonist bound conformation) clearly indicates that the protein induces the environment complementary to the distribution of the positive and negative potential of the ligand itself. Note that negatively charged Glu 705 in the WT protein or Asp 705 in the mutant are the primary sources of the negative potential at the position of the positively charged α-amino group of the ligand albeit not the only ones.

In the complex with the glutamate, as well as with other agonists, residues Glu 705 and Thr 480 are responsible for

the formation of a three-way hydrogen-bond network with the α-amino group of the glutamate ligand. This triangular network connects the two domains of the protein and is important for stabilizing the protein−ligand complex, e.g., glutaric acid in which α-amino group is absent does not bind to GluRs (*13*). The negative charge at protein position 705 in the E705D mutant is located further away from the binding site due to the shorter Asp side chain, thus destabilizing the amino group−protein interactions. In our simulations, however, reorganization of the waters residing in the binding pocket somewhat compensated for this deficiency via a newly formed hydrogen bond (compare Figure 4, panels a and b). Plasticity of the binding site, which allows for preserving the strength of the electrostatic interactions in the E705D mutant, also allowed for a tighter positioning of the ligand in the binding site, thus restricting its mobility and increasing the entropic penalty on binding ($T\Delta S$ term in eq 1). The overall result is decreased free energy of binding in the mutant, while the electrostatic interactions remain the same as in the WT protein.

The overall positive electrostatic potential in the binding cleft of the ligand-free protein found in our calculations (see Figure 5a and ref *16*) favors the binding of negatively charged ligands. In Figure 6, the positive potential extends far beyond the surface of the protein attracting negatively charged ligands. The long-range positive electrostatic potential of a protein may result in a so-called electrostatic steering (*50*), in which a negatively charged ligand diffuses randomly in solution until it reaches a region of space where it is attracted by the positive electrostatic field with the strength above 1 kT (corresponding to ca. 0.5 kcal/mol at room temperature). The ligand is then "steered" toward the protein along the increasing positive potential (as illustrated in Figure 6). Such a mechanism increases the relative concentration of negatively charged ligands in the vicinity of the protein, thus increasing the probability of binding.

Our study also includes an analysis of local ligand−protein interactions by calculating the asymmetric vibration of the carboxyl groups of the ligand. First, calculation of vibrational frequencies of the ligand allows us to validate our model by direct comparison with the FTIR experiment. Vibrational frequencies of carboxyl groups are known to be sensitive to electrostatic interactions and hydrogen bonds. Thus, through detailed analysis of the contribution of various protein and ligand subgroups, we can directly assess implications of the presence of various chemical groups and atoms in the vicinity of the ligand onto the ligand binding mechanism. Using such microscopic analysis, we have found strong evidence that the frequency shift observed in the E705D mutant can be attributed to the formation of a new hydrogen bond between Ser 654 and the ligand γ-carboxylate. The results of our spectroscopic calculations indicate that electrostatic interactions in the binding pocket of the glutamate receptor may play major role in the process of ligand binding. Frequency shifts upon removal of charged residues may serve as an accurate measure of the strength of the interaction between a protein residue and a ligand. For example, the removal of partial charges from the Arg 485 residue increases the frequency of ligand C_1OO^- asymmetric vibrations by 50−60 cm^{-1}. This result further supports the existence of strong interactions between this residue and the ligand.

Removing partial charges from the E705 residue, i.e., making it nonpolar, increased slightly the electrostatic binding energy of the ligand with the protein. This result contradicts the experimental observations made in mutation experiments (*10*, *13*) that showed that mutation of Glu 705 to Ala virtually abolished binding. One has to bear in mind that in our calculations the protein was in the closed conformation with the ligand locked in place and the dynamics of the ligand binding to the S1S2 protein, which requires initial recognition of the ligand and subsequent conformational rearrangement of the protein from its open to the closed conformation, has not been considered. Specifically localized negative charge of the E705 residue may serve during the first, initiating, step of the binding process to correctly position and orient the ligand. Such a mechanism is consistent with the earlier proposed "Venus flytrap" mechanism (*13*). It seems from our calculations that once the protein assumed its closed conformation with the ligand trapped inside the binding pocket that the stabilizing role of the position 705 becomes minimal. Further calculations are needed to test this hypothesis.

In summary, in this study we performed a detailed analysis of interaction of the GluR2 binding domain and its E705D mutant with the glutamate ligand in the closed conformation of the protein. The main goal of these simulations was to shed light on how protein residues and water molecules serve to accommodate the ligand in the binding site. Our combined free energy calculations and frequency shift calculations compared well with FTIR and microcalorimetry experiments performed previously on GluR2 and GluR4 proteins. Favorable comparison with existing experiments allows us to look in detail at the role of various interactions in the protein binding pocket. For example, strong interaction of the ligand with the Arg 485 residue manifests itself in both free energy calculations and large vibrational frequency shifts observed upon removal of this residue. The increased role of Ser 654 in E705D mutant has also been demonstrated via energetic and frequency calculations. One surprising result of this study was that removal of the charge from the 705 residue had a stabilizing effect on the electrostatic binding energy term and had only a small effect on the vibrational frequencies of the ligand carboxylates. We suggest that the main role of this residue is not in stabilization of the ligand in complex with the closed conformation of the protein (as simulated in this study) but rather in recognition and orientation of the ligand with respect to the open conformation of the protein in the early stages of the ligand binding. This hypothesis requires further investigation and will be the subject of our future work. Our calculations of electrostatic distribution produced by the protein in the binding pocket at the surface of the ligand establish clearly the existing charge complementarity of the binding pocket to its agonist ligand in the complex bound conformation. In the open conformation of the protein in the absence of the ligand, the electrostatic profile of the protein is very different with the positive potential extending far into solution and increasing strength toward the binding pocket to facilitate steering of a negatively charged ligand into the protein binding pocket. We have demonstrated that water molecules near the ligand γ-carboxyl group help stabilizing the glutamate molecule in the binding pocket. The observed formation of new hydrogen bonds and change in the geometry of water bridges in the mutant

provide additional information on nature of plasticity of the GluR2 binding site (previously known through its ability to accommodate a variety of ligands).

ACKNOWLEDGMENT

We thank Dr. V. Jayaraman for helpful discussions and sharing unpublished experimental data. Authors would like to thank our unknown reviewers for insightful comments that helped to significantly improve this study. Calculations reported in this study were in part made at Pittsburgh Supercomputer Center under the NSF PACI award.

REFERENCES

1. Hollmann, M., and Heinemann, S. (1994) Cloned glutamate receptors, *Annu. Rev. Neurosci. 17*, 31−108.
2. Dingledine, R., Borges, K., Bowie, D., and Traynelis, S. F. (1999) The glutamate receptor ion channels, *Pharmacol. Rev. 51*, 7−61.
3. Laube, B., Kuhse, J., and Betz, H. (1998) Evidence for a tetrameric structure of recombinant NMDA receptors, *J. Neurosci. 18*, 2954−2961.
4. Rosenmund, C., Stern-Bach, Y., and Stevens, C. F. (1998) The tetrameric structure of a glutamate receptor channel, *Science 280*, 1596−1599.
5. Krupp, J. J., Vissel, B., Heinemann, S. F., and Westbrook, G. L. (1998) N-terminal domains in the NR2 subunit control desensitization of NMDA receptors, *Neuron 20*, 317−327.
6. Chen, G.-Q., and Gouaux, E. (1997) Overexpression of a glutamate receptor (GluR2) ligand binding domain in *Escherichia coli*: application of a novel protein folding screen, *Proc. Natl. Acad. Sci. U.S.A. 94*, 13431−13436.
7. Armstrong, N., and Gouaux, E. (2000) Mechanisms for activation and antagonism of an AMPA-sensitive glutamate receptor: Crystal structures of the GluR2 ligand binding core, *Neuron 28*, 165−181.
8. Jin, R., and Gouaux, E. (2003) Probing the function, conformational plasticity, and dimer-dimer contacts of the GluR2 ligand-binding core: Studies of 5-substituted willardiines and GluR2 S1S2 in the crystal, *Biochemistry 42*, 5201−5213.
9. Armstrong, N., Sun, Y., Chen, G.-Q., and Gouaux, E. (1998) Structure of a glutamate receptor ligand-binding core in complex with kainate, *Nature 395*, 913−917.
10. Lampinen, M., Pentikainen, O., Johnson, M. S., and Keinanen, K. (1998) AMPA receptors and bacterial periplasmic amino acid-binding proteins share the ionic mechanism of ligand recognition, *EMBO J. 17*, 4704−4711.
11. Kuusinen, A., Arvola, M., and Keinanen, K. (1999) Oligomerization and ligand-binding properties of the ectodomain of the α-amino-3-hydroxy-5-methyl-4-isoxazole propionic acid receptor subunit GluRD, *J. Biol. Chem. 274*, 28937−28943.
12. Deming, D., Cheng, Q., and Jayaraman, V. (2003) Is the isolated ligand binding domain a good model of the domain in the native receptor? *J. Biol. Chem. 278*, 17589−17592.
13. Abele, R., Keinanen, K., and Madden, D. R. (2000) Agonist-induced isomerization in a glutamate receptor ligand-binding domain. A kinetic and mutagenetic analysis, *J. Biol. Chem. 275*, 21355−21363.
14. Arinaminpathy, Y., Sansom, M. S. P., and Biggin, P. C. (2002) Molecular dynamics Simulations of the ligand binding domain of the ionotorpic glutamate receptor GluR2, *Biophys. J. 82*, 676−683.
15. Kubo, M., Odai, K., Sugimoto, T., and Ito, E. (2001) Quantum chemical study of agonist-receptor vibrational interactions for activation of the glutamate receptor, *J. Biochem.* (Tokyo). *129*, 869−874.
16. Kubo, M., Shiomitsu, E., Odai, K., Sugimoto, T., Suzuki, H., and Ito, E. (2003) Quantum chemical study of ligand−receptor electrostatic interactions in molecular recognition of the glutamate receptor, *J. Mol. Struct.634*, 145−157.
17. Kubo, M., Shiomitsu, E., Odai, K., Sugimoto, T., Suzuki, H., and Ito, E. (2003) Agonist-specific vibrational excitation of glutamate receptor, *J. Mol. Struct. 639*, 117−128.
18. Kubo, M., Shiomitsu, E., Odai, K., Sugimoto, T., Suzuki, H., and Ito, E. (2004) Picosecond dynamics of the glutamate receptor in response to agonist-induced vibrational excitation, *Proteins: Struct., Funct., Genet. 54*, 231−236.
19. Mendieta, J., Ramirez, G., and Gago, F. (2001) Molecular dynamics simulations of the conformational changes of the glutamate receptor ligand-binding core in the presence of glutamate and kainate, *Proteins: Struct., Funct., Genet. 44*, 460−469.
20. Kubo, M., and Ito, E. (2004) Structural dynamics of an ionotropic glutamate receptor, *Proteins: Struct., Funct., Bioinf. 56*, 411−419.
21. Berman, H. M., Westbrook, J., Feng, Z., Gilliland, G., Bhat, T. N., Weissig, H., Shindyalov, I. N., and Bourne, P. E. (2000) The Protein Data Bank, *Nucleic Acids Res. 28*, 235−242.
22. Honig, B., Sharp, K., and Yang, A. S. (1993) Macroscopic Models of aqueous-solutions − biological and chemical applications, *J. Phys. Chem. 97*, 1101−1109.
23. Kurnikov, I. V., Ratner, M. A., and Pacheco, A. A. (2005) Redox equilibria in hydroxylamine oxidoreductase. Electrostatic control of electron redistribution in multielectron oxidative processes, *Biochemistry 44*, 1856−1863.
24. Antosiewicz, J., Mccammon, J. A., and Gilson, M. K. (1994) Prediction of pH-dependent properties of proteins, *J. Mol. Biol. 238*, 415−436.
25. Singh, U. C. (1984) An approach to computing electrostatic charges for molecules, *J. Comput. Chem. 5*, 129−145.
26. Besler, B. H. (1990) Atomic charges derived from semiempirical methods, *J. Comput. Chem. 11*, 431−439.
27. Jin, R., Horning, M., Mayer, M., and Gouaux, E. (2002) Mechanism of activation and selectivity in a ligand-gated ion channel: Structural and functional studies of GluR2 and quisqualate, *Biochemistry 41*, 15635−15643.
28. Kurnikov, I. V. (2003) *HARLEM*, biomolecular simulation program, http://www.kurnikov.org/harlem_main.html.
29. Ryckaert, J.-P., Ciccotti, G., and Berendsen, H. J. C. (1977) Numerical integration of the Cartesian equations of motion of a system with constraints: Molecular dynamics of *n*-alkanes. *J. Comput. Phys. 23*, 327−341.
30. Case, D. A., Pearlman, D. A., Caldwell, J. W., Cheatham III, T. E., Ross, W. S., Simmerling, C. L., Darden, T. A., Merz, K. M., Stanton, R. V., Cheng, A. L., Vincent, J. J., Crowley, M., Tsui, V., Radmer, R. J., Duan, Y., Pitera, J., Massova, I., Seibel, G. L., Singh, U. C., and Kollman, P. A. (1999). *AMBER 6*, University of California, San Francisco.
31. Cornell, W. D., Cieplak, P., Bayly, C. I., Gould, I. R., Merz, K. M., Ferguson, D. M., Spellmeyer, D. C., Fox, T., Caldwell, J. W., and Kollman, P. A. (1995) A second generation force field for the simulation of proteins, nucleic acids, and organic molecules, *J. Am. Chem. Soc. 117*, 5179−5197.
32. Kollman, P. A., Massova, I., Reyes, C., Kuhn, B., Huo, S. H., Chong, L., Lee, M., Lee, T., Duan, Y., Wang, W., Donini, O., Cieplak, P., Srinivasan, J., Case, D. A., and Cheatham, T. E. (2000) Calculating structures and free energies of complex molecules: Combining molecular mechanics and continuum models, *Acc. Chem. Res. 33*, 889−897.
33. Kalra, P., Reddy, T. V., and Jayaram, B. (2001) Free energy component analysis for drug design: A case study of HIV-1 protease-inhibitor binding, *J. Med. Chem. 44*, 4325−4338.
34. Bryce, R. A., Hillier, I. H., and Naismith, J. H. (2001) Carbohydrate-protein recognition: molecular dynamics simulations and free energy analysis of oligosaccharide binding to concanavalin A, *Biophys. J. 81*, 1373−1388.
35. Hou, T., Guo, S., and Xu, X. (2002) Predictions of binding of a diverse set of ligands to gelatinase-A by a combination of molecular dynamics and continuum solvent models, *J. Phys. Chem. B 106*, 5527−5535.
36. Mamonov, A. B., Coalson, R. D., Nitzan, A., and Kurnikova, M. G. (2003) The role of the dielectric barrier in narrow biological channels: A novel composite approach to modeling single-channel currents, *Biophys. J. 84*, 3646−3661.
37. Le Grand, S. M., and Merz, J. (1993) Rapid approximation to molecular surface area via the use of Boolean logic and look-up tables, *J. Comput. Chem. 14*, 349−352.
38. Honig, B., and Nicholls, A. (1995) Classical electrostatics in biology and chemistry, *Science 268*, 1144−1149.
39. Swanson, J. M. J., Henchman, R. H., and McCammon, J. A. (2004) Revisiting free energy calculations: A theoretical connection to MM/PBSA and direct calculation of the association free energy, *Biophys. J. 86*, 67−74.

40. Luo, H. B., and Sharp, K. (2002) On the calculation of absolute macromolecular binding free energies, *Proc. Natl. Acad. Sci. U.S.A. 99*, 10399−10404.
41. Nakamoto, K. (1997) *Infrared and Raman Spectra of Inorganic and Coordination Compounds*, Wiley, New York.
42. Laberge, M., Sharp, K. A., and Vanderkooi, J. M. (1998) Effect of charge interactions on the carboxylate vibrational stretching frequency in c-type cytochromes investigated by continuum electrostatic calculations and FTIR spectroscopy, *Biophys. Chem. 71*, 9−20.
43. Speranskiy, K., and Kurnikova, M. (2004) Accurate theoretical prediction of vibrational frequencies in an inhomogeneous dynamic environment: a case study of a glutamate molecule in water solution and in a protein-bound form, *J. Chem. Phys. 121*, 1516−1524.
44. Frisch, M. J., Trucks, G. V., Schlegel, H. B., Scuseria, M. A. Robb, Cheeseman, J. R., Zakrzewski, V. G., Montgomery, J. A., Stratmann, R. E., Burant, J. C., Dapprich, S., Millam, J. M., Daniels, A. D., Kudin, K. N., Strain, M. C., Farkas, O., Tomasi, J., Barone, V., Cossi, M., Cammi, R., Mennucci, B., Pomelli, C., Adamo, C., Clifford, S., Ochterski, J., Petersson, G. A., Ayala, P. Y., Cui, Q., Morokuma, K., Malick, D. K., Rabuck, A. D., Raghavachari, K., Foresman, J. B., Cioslowski, J., Ortiz, J. V., Stefanov, B. B., Liu, G., Liashenko, A., Piskorz, P., Komaromi, I., Gomperts, R., Martin, R. L., Fox, D. J., Keith, T., Al-Laham, M. A., Peng, C. Y., Nanayakkara, A., Gonzalez, C., Challacombe, M., Gill, P. M. W., Johnson, B. G., Chen, W., Wong, M. W., Andres, J. L., Head-Gordon, M., Replogle, E. S., and Pople, J. A. (1998) *Gausssian 98*, Gaussian, Inc.; Pittsburgh, PA.
45. Scott, A. P., and Radom, L. (1996) Harmonic vibrational frequencies: An evaluation of Hartree- Fock, Moller−Plesset, quadratic configuration interaction, density functional theory, and semiempirical scale factors, *J. Phys. Chem. 100*, 16502−16513.
46. Jayaraman, V., Keesey, R., and Madden, D. R. (2000) Ligand-protein interactions in the glutamate receptor, *Biochemistry 39*, 8693−8697.
47. Cheng, Q., Thiran, S., Yernool, D., Gouaux, E., and Jayaraman, V. (2002) A vibrational spectroscopic investigation of interactions of agonists with GluR0 a prokaryotic glutamate receptor, *Biochemistry 41*, 1602−1608.
48. Jayaraman, V. (2002) University of Texas Health Science Center, Houston, Texas, personal communication.
49. Kawamoto, S., Uchino, S., Xin, K. Q., Hattori, S., Hamajima, K., Fukushima, J., Mishina, M., and Okuda, K. (1997) Arginine-481 mutation abolishes ligand-binding of the AMPA-selective glutamate receptor channel a1-subunit, *Mol. Brain Res. 47*, 339−344.
50. Tan, R. C., Truong, T. N., McCammon, J. A., and Sussman, J. L. (1993) Acetylcholinesterase − electrostatic steering increases the rate of ligand-binding, *Biochemistry 32*, 401−403.

BI050547W